Hashemi & Visser *New Zealand Journal of Forestry Science* (2026) 56:10
https://doi.org/10.33494/nzjfs562026x528x
E-ISSN: 1179-5395
published on-line: 25/07/2026

Research Article **Open Access**

New Zealand Journal of Forestry Science

Estimating a geotechnical factor of safety: A Python-based workflow for regional landslide susceptibility assessment

Mahsa Hashemi* and Rien Visser

New Zealand School of Forestry, University of Canterbury, Private Bag 4800, Christchurch 8140, New Zealand

*Corresponding author: mahsa.hashemi@pg.canterbury.ac.nz

(Received for publication 20 February 2026; accepted in revised form 15 July 2026)

Editor: Karen Bayne

Abstract

Background: Assessing slope stability using geotechnical engineering principles typically uses a Factor of Safety (FS) to define the ratio of resisting to driving forces along a potential failure surface of landslides. Accurate estimation of this FS is central to evaluating shallow landslide susceptibility, yet field-based measurements of soil strength are rarely available across steep, remote terrain. This challenge is particularly evident in New Zealand's erodible hill-country. To address this limitation, this study developed a reproducible Python-based workflow for computing FS using environmental geographic information system (GIS) layers and published geotechnical parameters, without requiring in-situ testing.

Methods: To demonstrate the efficacy of the method, a case study area was selected in Gisborne, New Zealand. In this region, major storms triggered numerous shallow landslides in a plantation forest area that was later accurately mapped by forest owners. Geological and soil units were assigned representative shear-strength properties using values compiled from national datasets and previous studies. Terrain variables, including slope, curvature, elevation, drainage metrics, soil attributes, and rainfall, were extracted at 42,000 landslide and non-landslide sample locations. Landslide samples were derived from the centroids of 22,000 mapped shallow landslide polygons, representing about 4,400 ha of documented landslide-affected terrain. Non-landslide samples were generated using a terrain-constrained random sampling approach within the same study area, explicitly excluding mapped landslide polygons and non-terrestrial areas. An infinite-slope model was implemented in Python to compute FS under a range of hydrological and soil-depth scenarios.

Results: For this case study area, the median FS across the dataset was 1.3, and approximately 28% of samples fell below the instability threshold (FS < 1). Sensitivity analysis confirmed that FS was strongly responsive to increasing saturation ratio and moderately affected by soil depth. A qualitative comparison with mapped landslides showed that unstable and near-critical conditions were more frequently associated with inventoried failure locations, with 37% of landslide samples exhibiting FS < 1 compared to 18% of non-landslide reference points.

Conclusions: The results demonstrate that a transparent, Python-based workflow can generate physically interpretable FS estimates suitable for regional-scale screening in data-limited environments. The workflow establishes a foundation for future hybrid models in which FS-derived indicators can support, constrain, or enhance machine-learning frameworks of landslide susceptibility.

Keywords: Geotechnical parameters; GIS; hydrological saturation; infinite slope model; New Zealand hill-country; regional susceptibility assessment; shallow landslides; soil depth uncertainty.

Introduction

Landslides are among the most widespread geomorphic hazards worldwide, generating substantial economic, environmental, and ecological impacts in mountainous terrain (Petley 2012; Froude & Petley 2018). In New Zealand, shallow landslides are particularly prevalent during intense rainfall events (Marden 2012; Phillips et al. 2012), especially where steep hillslopes are underlain by weak, highly weathered sedimentary units. These failures are prominent in the highly erodible Tertiary mudstone and siltstone hill-country of the Gisborne, New Zealand, where repeated storm events have highlighted the importance of lithology in controlling shallow mass movement (Marden et al. 2023). Such failures contribute to elevated sediment loads, soil loss, and repeated infrastructure damage within plantation forests, reinforcing the need for regional-scale assessments that support land-management, forestry planning and infrastructure placement, and slope stability risk management (Smith et al. 2023; Phillips et al. 2024). In plantation forestry environments, shallow landslides can directly affect road networks, harvest planning, and operational safety, making reliable terrain stability assessment important for decision-making (Smith et al. 2024).

A central metric for evaluating slope stability is the FS, defined as the ratio of resisting to driving forces along a potential failure surface (Skempton & DeLory 1957; Sharma 2002). While FS < 1 indicates potential failure, accurate estimation requires knowledge of soil strength, hydrological conditions, and subsurface geometry. Obtaining such measurements across large, remote regions is often infeasible, particularly in steep-slope forestry landscapes. Therefore, there is growing interest in workflows that compute FS using GIS-derived variables and published geotechnical parameters, reducing the need for site-specific field investigations (Pack et al. 1998; Chae et al. 2017).

Physically based slope-stability models provide a mechanistic representation of shallow landslide processes by quantifying the balance between shear stress and shear strength (Wu & Sidle 1995; Iverson 2000). A range of physically based and semi-empirical models have been developed for regional landslide susceptibility assessment, including SHALSTAB, SINMAP, and TRIGRS, each differing in complexity, data requirements, and hydrological representation (Montgomery & Dietrich 1994; Pack et al. 1998; Baum et al. 2008; Hashemi & Visser 2026).

The infinite-slope model was selected for this study because it is suitable for regional screening due to its conceptual simplicity and compatibility with raster-based geospatial workflows (Montgomery & Dietrich 1994; Pack et al. 1998; Baum et al. 2008). Its key inputs are effective cohesion (c'), internal friction angle (ϕ'), unit weight (γ), soil depth (z), and hydrological saturation ratio (s), can be approximated using published geotechnical parameter ranges when field measurements are unavailable (Carter & Bentley 1991; Look 2007).

Advances in national geospatial databases in New Zealand, including QMAP geology, S-map soils, National Institute of Water and Atmospheric Research (NIWA) rainfall surfaces, and high-resolution Digital Elevation Models (DEMs) derived from Land Information New Zealand (LINZ) national elevation datasets, now make it feasible to derive these inputs programmatically across large areas of New Zealand. These developments have increased interest in applying physically based FS modelling as a practical tool for regional-scale slope-stability assessment in data-limited environments.

With these advances, two persistent challenges limit the accuracy of large-scale FS estimation. First, hydrological conditions are often oversimplified, with many studies assuming spatially uniform or steady-state saturation despite strong storm-driven variability (Baum et al. 2010; Sidle & Bogaard 2016). Second, geotechnical parameters are often associated with significant uncertainty and may not capture lithology-specific variability at regional scale (Fiolleau et al. 2022; Ye et al. 2025).

A recent review highlights the need for transparent, reproducible workflows that derive input parameters systematically from published sources and geological descriptions (Dahal & Lombardo 2024). Hybrid approaches in landslide susceptibility modelling are increasingly combining physically based understanding with data-driven methods (Dahal & Lombardo 2024; Pei & Qiu 2024; Wang et al. 2024). In this context, FS-derived indicators can serve as physically meaningful features that support and enhance machine-learning models. The workflow developed in this study provides a transparent and scalable framework for generating such physics-based inputs, offering a foundation for future hybrid modelling applications.

This study addresses that need, using New Zealand's steep, forested hill-country as a test environment. The objectives are to:

1. Develop a reproducible, Python-based workflow for calculating a FS estimate without field measurements;
2. For a case study area, systematically assign geotechnical and hydrological parameters to lithological units using national datasets and published values;
3. Through analyses of the results, assess the efficacy of the model and spatial patterns of the FS estimate to evaluate its potential as a practical, physically interpretable indicator for regional landslide susceptibility screening.

Methods

Factor of Safety for shallow landslides

This study develops a reproducible Python-based workflow for estimating a geotechnical FS for shallow landslides using national-scale geological, soil, hydrological, and topographic datasets. The FS computed uses the infinite-slope model originally formulated by Skempton and DeLory (1957), whereby this calculation remains a common standard and is widely used in both geotechnical engineering and physically based landslide modelling (Montgomery & Dietrich 1994; Iverson 2000; Duncan et al. 2014; Hungr et al. 2014).

$$FS = (c' + (\gamma z\cos^2\theta - s\,\gamma_w z\cos^2\theta)\tan\phi') \,/\, \gamma z\sin\theta\cos\theta$$

where:

- c' is the effective cohesion (kPa),
- ϕ' is the internal friction angle (degrees),
- γ is the unit weight of soil (kN/m^3),
- γ_w is the unit weight of water (9.81 kN/m^3),
- z is the assumed failure depth (m),
- θ is the slope angle (degrees), and
- s is the saturation ratio (dimensionless, 0–1).

Workflow Overview

Figure 1 shows the primary workflow developed for the FS for Shallow Landslides Model. The workflow presented in Figure 1 can be broken down into five main steps:

Step 1: Data Acquisition and Preprocessing

A suite of national-scale geospatial datasets was used to parameterise the FS model (Table 1). All raster and vector layers were projected to New Zealand Transverse Mercator (NZTM2000, EPSG:2193) and resampled/aligned to the 8 m DEM. Each dataset contributed to a specific component of the infinite-slope model, topography, material strength, hydrology, or external forcing (rainfall).

For the topographic data, obtained from the LINZ DEM, an 8 m DEM provided the geometric basis for slope angle (θ), aspect, curvature, and other terrain metrics, derived using WhiteboxTools and rasterio (Lindsay 2016). The lithological polygons were extracted from QMAP (scale 1:250,000) and reclassified into geotechnical groups through Python text-parsing rules. Each lithology group was assigned representative ranges of effective cohesion, friction angle, and unit weight from Carter & Bentley (1991) and Look (2007). This approach is consistent with regional characterisations of East Coast hill-country terrain, where highly weathered Tertiary mudstone units are widely recognised as being prone to shallow landsliding under intense rainfall (Marden et al. 2023).

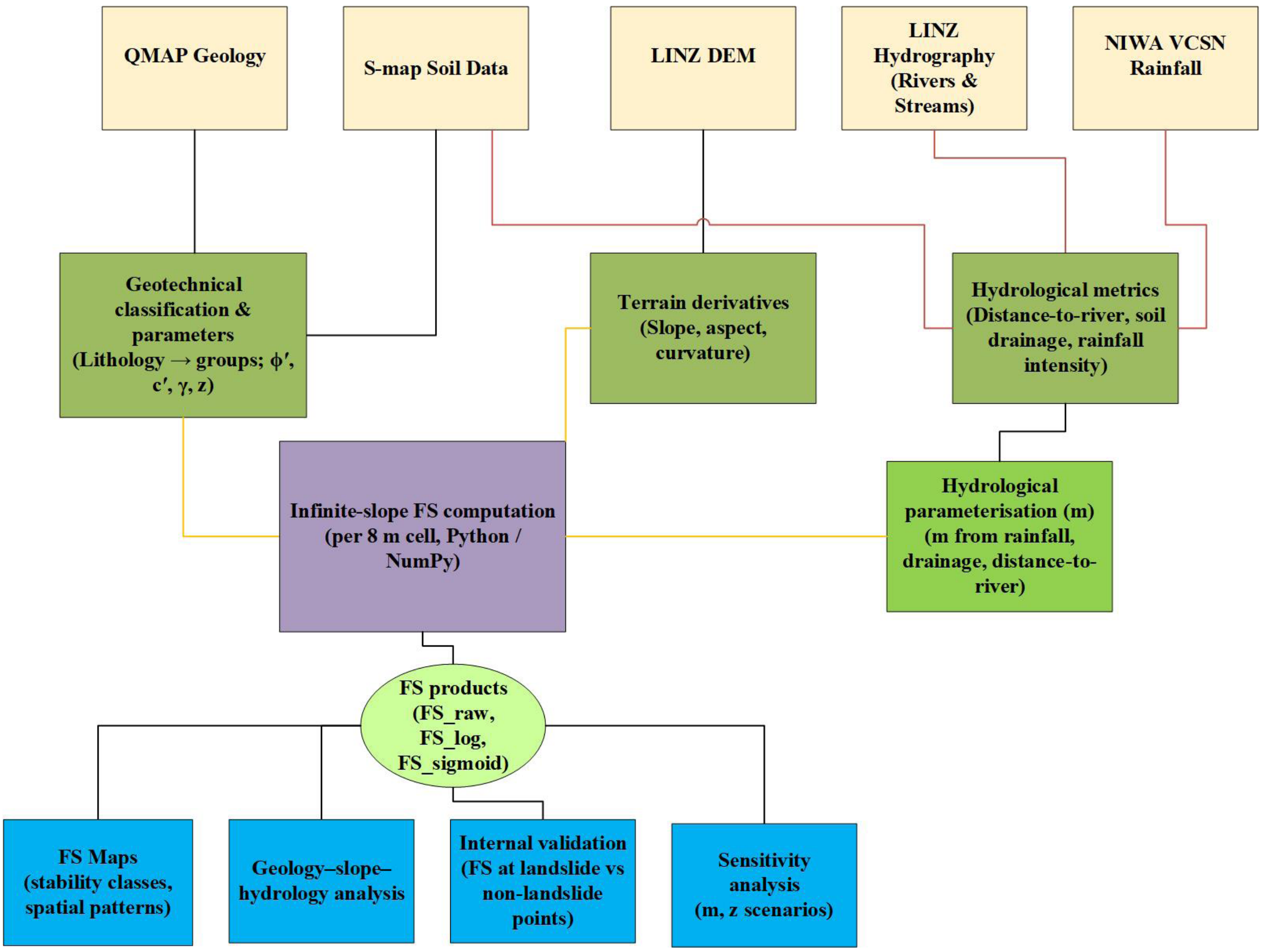

FIGURE 1. Python-based workflow for Factor of Safety computation for shallow landslide susceptibility assessment.

TABLE 1: Summary of datasets used for determining a geotechnical Factor of Safety

Dataset	Source	Spatial resolution / scale	Role in FS model
Digital Elevation Model (DEM)	Land Information New Zealand (LINZ) – National DEM	8 m grid	Derivation of slope (θ), aspect, curvature, and local relief for geometric stability terms
Geological map (QMAP)	GNS Science 1:250 000 Geological Map of New Zealand	Polygon (lithological units)	Base layer for lithological and geotechnical class assignment (ϕ', c', γ)
Soil dataset (S-map)	Landcare Research New Zealand	Vector polygons (national)	Provides soil texture, drainage class, and approximate depth (z)
Hydrology	LINZ Hydrography Dataset	Vector (streams & rivers)	Used to compute distance-to-river and infer groundwater proximity (s)
Rainfall data	NIWA Virtual Climate Station Network (VCSN)	~5 km grid (interpolated climate surface)	Provides mean annual and event-based rainfall for estimating saturation ratio (s)
Landslide inventory	GNS Science National Landslide Database + Gisborne District Council imagery (2023 LiDAR)	Points / polygons	Used only for validation of FS and susceptibility maps

S-map (Manaaki Whenua - Landcare Research New Zealand; Lilburne et al. 2012) provided soil drainage class, texture, and indicative soil depth. Drainage class contributed to hydrological estimation of saturation ratio (s), while soil texture supported the assignment of geotechnical parameter ranges for sedimentary and volcanic units. Distance to the nearest river/stream was computed using Euclidean distance and used as a proxy for subsurface saturation potential, based on the LINZ Hydrography layer. Finally, mean annual and storm-related rainfall fields were extracted from VCSN (NIWA) and resampled to 8 m to align with the DEM. Rainfall quantiles informed the hydrological classification for estimating s.

Step 2: Geotechnical Classification and Parameter Assignment

The abstraction step was introduced to enable consistent and scalable assignment of geotechnical parameters across heterogeneous lithological units at regional scale, where site-specific measurements are unavailable. Each geotechnical class represents characteristic strength and drainage behaviour and was used exclusively for parameterisation within the infinite-slope stability model (Table 2).

Classification was implemented using a hierarchical, keyword-based text-parsing system applied to QMAP lithology descriptions. Diagnostic terms were identified programmatically (case-insensitive) and mapped to predefined geotechnical classes based on their expected mechanical and hydrological behaviour. Examples include:

- "mudstone", "siltstone", "argillite" → soft mudstone / siltstone
- "sandstone", "greywacke", "torlesse" → sandstone / greywacke
- "alluvium", "colluvium", "fan", "gravel" → colluvium / alluvium
- "ash", "tephra", "ignimbrite", "pumice" → volcanic ash / tephra
- "basalt", "andesite", "gabbro" → strong volcanic / basaltic rocks

Where multiple descriptors occurred within a single lithology, priority was consistently assigned to the weaker or more failure-prone component (e.g., "weathered" overriding "bedrock", "mudstone" overriding "sandstone", and "colluvium" overriding underlying bedrock). Lithologies with ambiguous or generic descriptions were assigned to conservative fallback groups to ensure full parameter coverage.

For result interpretation, the geotechnical classes defined above are reported at a finer material-descriptor level derived from the refined QMAP text classification at the sample-point locations (e.g., weathered rock, brecciated rock, sand, stiff clay, soft clay, volcanic ash, pumice). These material descriptors represent dominant near-surface expressions within each geotechnical class and are used to improve geological interpretability of mapped FS patterns, while the underlying parameterisation remains consistent with the geotechnical groupings.

Table 2 summarises the representative parameter ranges for each geotechnical class based on literature-derived values. All parameters were standardised to consistent engineering units and joined to QMAP polygons prior to rasterisation. Soil depth (z) for the baseline FS computation was set to values consistent with documented shallow failure-plane depths in New Zealand hill-country (typically 1-2 m; Marden & Rowan 1993), with additional depth scenarios explored in sensitivity analysis.

TABLE 2: Representative geotechnical parameter ranges assigned to lithology groups for using in the FS model.

Lithology Group	Cohesion c' (kPa)	Friction Angle ϕ' (°)	Unit Weight γ (kN/m^3)	Baseline Soil Depth z (m)
Soft mudstone / siltstone	5–15	18–22	18–20	1–1.5
Sandstone / Greywacke	10–25	25–30	19–21	1–2
Colluvium / Alluvium	3–10	20–26	17–19	1–1.5
Volcanic ash / tephra	2–8	28–32	15–18	0.8–1.2
Strong greywacke / basalt	20–40	30–38	21–23	1.5–2

The parameter ranges were primarily derived from standard geotechnical reference tables and correlations (Carter & Bentley 1991; Look 2007) and adapted to represent typical lithological conditions in the study area.

Step 3: Hydrological Parameter Estimation

Hydrological conditions were represented using the dimensionless saturation ratio (s), defined as the ratio of saturated soil height to total soil depth (h/z), following the steady-state formulation widely used in SHALSTAB and related infinite-slope models. Because direct pore-pressure or groundwater measurements were not available, s was estimated using geospatial proxies derived from rainfall accumulation and drainage proximity, an approach consistent with previous regional-scale hydrological modelling (Montgomery & Dietrich 1994; Pack et al. 1998).

Mean annual precipitation was obtained from the NIWA (VCSN; Tait et al. 2006) and resampled to the 8 m DEM grid. Distance to the nearest river or stream was calculated from the LINZ Hydrography dataset, as cells closer to drainage channels typically exhibit higher pore-pressure potential due to lateral throughflow and topographic convergence (Beven & Kirkby 1979; O'Loughlin 1986; Montgomery & Dietrich 1994).

To operationalise these relationships, a rule-based Python classification scheme was applied to assign s values using rainfall quantiles and distance-to-river thresholds (Table 3). Assigned s values ranged between 0.3 and 1, representing dry-to-moderately moist through fully saturated conditions commonly observed in New Zealand hill-country terrain (Look 2007). A minimum value of s = 0.3 was adopted to reflect the rarity of completely dry conditions during periods associated with shallow landslide occurrence in New Zealand. This approach captures broad spatial patterns in saturation potential without requiring detailed transient hydrological data, which are necessary for more complex infiltration models such as TRIGRS (Baum et al. 2008).

The resulting s raster was combined with geotechnical and topographic layers to compute FS across the study area using the infinite-slope model. This quasi-steady-state assumption is appropriate for regional screening of rainfall-triggered shallow landslides in New Zealand's hill-country terrain, where failure is typically governed by rapid saturation of shallow soil mantles rather than slow, deep groundwater responses (Phillips et al. 2012; Sidle & Bogaard 2016).

Step 4: Factor of Safety calculation and transformation

The raw FS output of the infinite-slope model preserves full physical meaning and is suitable for mapping and threshold-based interpretation (e.g., FS < 1). To improve the usability of FS outputs for subsequent analysis and interpretation, two transformed variants of FS were generated. These transformations were designed to support statistical characterisation of FS distributions and facilitate comparative spatial visualisation across the study area.

Log-transformed FS: To reduce extreme right-skewness caused by very high FS values in low-slope or highly stable areas, a logarithmic transformation was applied:

$$FS_{log} = \log(1+FS)$$

This transformation moderates long-tailed distributions and improves numerical stability for summary statistics and comparative analyses.

Sigmoid-scaled FS: To compress the wide range of FS values into a bounded interval while preserving relative spatial contrasts, FS was rescaled using a logistic (sigmoid) transformation:

$$FS_{sigmoid} = 1/(1+\exp(-FS)$$

TABLE 3: Assignment of saturation ratio (s) using rainfall and drainage proxies in the FS model.

Rainfall–drainage condition	Distance to river (m)	Mean annual rainfall (mm)	Assigned s value	Hydrological interpretation
Very high wetness	< 50	> 2500	1	Fully saturated (h/z = 1)
High wetness	50–200	2000–2500	0.8	Near saturated
Moderate wetness	200–500	1500–2000	0.5	Partially saturated
Low wetness	> 500	< 1500	0.3	Unsaturated / relatively dry

The rescaling maps FS values into the (0, 1) interval, facilitating visual comparison between areas of differing stability while retaining monotonic correspondence with the original FS values. All three FS representations (FS_raw, FS_log, FS_sigmoid) were exported as GeoTIFF raster layers and extracted at sample-point locations to support statistical analysis, mapping, and interpretation of regional slope-stability patterns.

Case Study Data

A comprehensive GIS dataset of mapped shallow landslides was provided for this case study by a New Zealand forest company in the Tairawhiti region, East Coast of the North Island. These shallow landslides occurred in their estate following major storms in 2023. The landslide samples information required for this method were derived from the centroids of mapped shallow landslide polygons (~22,000 points), representing approximately 4,400 ha of documented landslide-affected terrain.

Non-landslide samples were generated within the same spatial domain using a physics-informed, terrain-constrained random sampling approach. Sampling was restricted to areas outside all mapped landslide polygons and non-terrestrial surfaces and preferentially focused on terrain expected to be mechanically stable under typical conditions (e.g., lower slope gradients and greater distance from drainage channels). FS was computed at approximately 42,000 sample locations distributed across the full spatial extent of a plantation forestry estate in the Gisborne, New Zealand.

A qualitative overlay of areas with FS < 1 and the labelled landslide points in the dataset was used as an internal consistency check. This comparison assessed whether locations identified as landslides in the compiled dataset aligned with low-FS areas generated by the Python-based workflow. The check did not influence FS computation and was used solely to confirm that the model produced physically plausible stability patterns for known failure locations.

Step 5: Sensitivity analysis

To evaluate the robustness and physical consistency of the literature-derived FS estimates, sensitivity analysis should be carried out focusing on key parameters that exert dominant control on infinite-slope stability. Because the workflow relies on national datasets and published geotechnical ranges rather than site-specific field measurements, assessing the response of FS to uncertainty in assumed hydrological and geometric conditions is essential for interpreting the reliability of the results at regional scale.

For this case study data, analysis concentrated on two parameters that strongly influence shallow landslide initiation being (i) the hydrological saturation ratio (s), which modulates pore-water pressure and effective stress, and (ii) soil depth (z), which governs both driving and resisting forces within the soil mantle (Montgomery & Dietrich 1994; Iverson 2000). Mechanical strength parameters (effective cohesion c' and friction angle φ') were held constant during this analysis to maintain comparability across scenarios and to isolate the effects of hydrological loading and soil thickness, which are typically the most uncertain inputs in regional-scale applications.

Nine sensitivity scenarios were constructed using all combinations of three saturation states and three soil-depth assumptions:

- Saturation ratio: s = 0, 0.5, 1
- Soil depth: z = 0.5, 1, 1.5 m

These ranges were selected to represent dry to fully saturated conditions and commonly reported shallow failure depths in New Zealand hill-country terrain. For each (s, z) combination, FS was recomputed at all sample locations, including both landslide-derived and non-landslide reference points distributed across the full spatial extent of the study area.

Results

The workflow developed, using the GIS- and literature-derived infinite-slope model, produced continuous FS estimates for all evaluated raster-derived sample points across the study area. The spatial distribution of raw FS values (FS_raw) shown in Figure 2 provides an initial regional-scale context, illustrating broad contrasts between lower-stability terrain on steep, dissected hillslopes and higher stability conditions on gentle slopes and ridge tops. In the sample area shown, lower FS values dominate steep, dissected hillslopes, while higher FS values occur on gentle slopes, ridge tops, and low-relief terrain. Concentration of low FS values along convergent hollows and drainage lines are also visible.

The mapped FS field shows spatial patterns across the study area. Lower FS values form continuous belts over the dissected hill country, particularly in the northern and central parts of the region, whereas higher FS values occur more frequently on gentle slopes, coastal terraces, and around broad interfluves. This transition from predominantly low FS in steep terrain to higher FS on subdued topography is consistent with the control of slope angle and curvature in the infinite-slope formulation.

To highlight these spatial contrasts in a form suitable for regional interpretation, FS was grouped into three stability classes and visualised alongside the drainage network (Figure 3). Areas classified as unstable (FS < 1) form narrow, elongated zones along valley sides and within deeply incised terrain, while stable areas (FS > 1.5) dominate ridge tops, convex slope positions, and lower-relief areas. Intermediate FS values (1-1.5) commonly occur as transition bands between stable and unstable terrain, outlining the margins of steep hollows and headwater catchments.

When viewed together with the river and stream network (Figure 3), unstable terrain shows a strong tendency to cluster close to channels and along convergent flow paths. Many of the lowest FS values follow the main drainage lines and their tributaries, whereas stable terrain is more prevalent at greater distances from the network. The inset in Figure 3 further

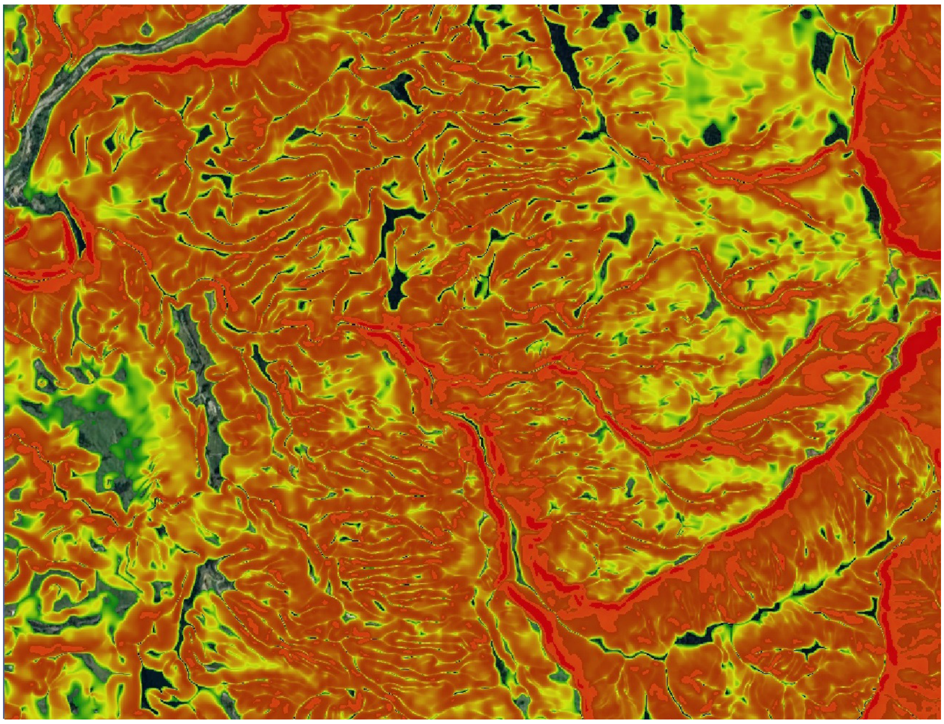

FIGURE 2: Raw Factor of Safety (FS_raw) for a sample section of the study area, showing the continuous spatial distribution of slope stability.

illustrates the local-scale relationship between low FS zones and mapped landslides within a representative headwater catchment. This spatial association between low FS values and proximity to drainage channels is consistent with the hydrological assumptions of the infinite-slope framework and with field observations of shallow landslides concentrating in saturated hollows and incised headwater valleys in New Zealand hill-country.

The distribution of raw FS values (FS_raw) is strongly right-skewed (Figure 4a), with most samples falling within FS ≈ 0.5–3 and a long upper tail extending beyond

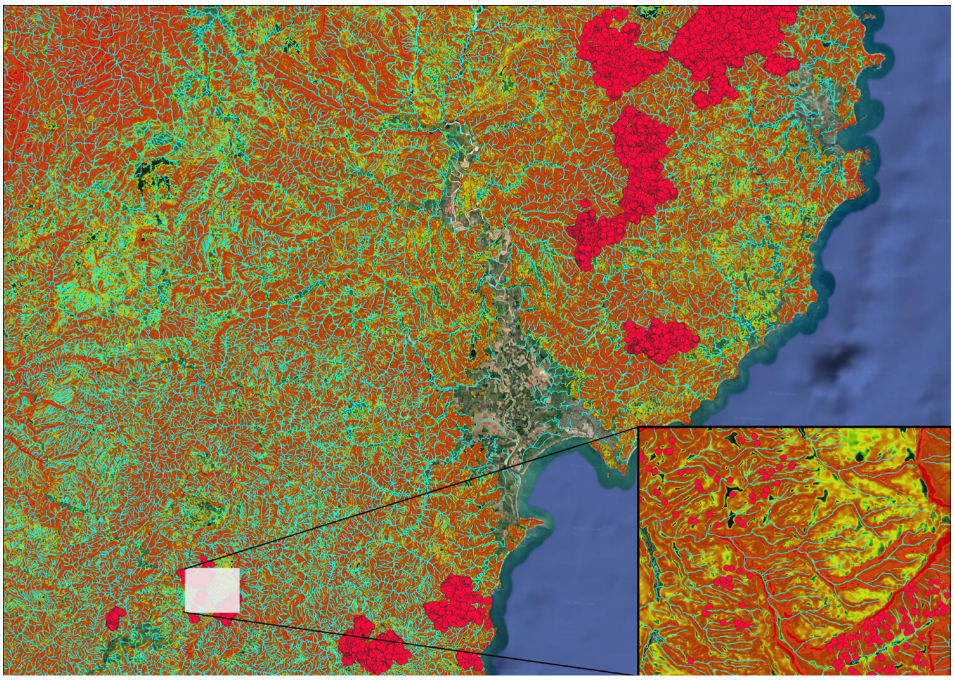

FIGURE 3. FS distribution overlaid with the drainage network

FS > 10. This behaviour reflects the expected contrast between steep slopes underlain by weaker sedimentary materials and more stable landscape positions such as ridge crests, low-gradient terrain, and areas underlain by stronger lithologies. Across the full dataset, the median FS was 1.30 and the mean FS was 2.63, indicating the presence of a relatively small number of highly stable locations that elevate the overall average. Approximately 28% of all samples exhibited FS < 1 under the modelled hydrological condition, while the remaining values were distributed between moderately stable terrain (1 ≤ FS ≤ 1.5) and clearly stable conditions (FS > 1.5).

To reduce the influence of extreme high FS values for evaluation, a logarithmic transformation was applied. The log-transformed FS (FS_log) substantially compressed the right tail of the distribution and produced a more compact, approximately symmetric form (Figure 4b), drawing very large FS values closer to the centre of the distribution. A sigmoid transformation (FS_sigmoid) was also applied to map FS values onto the interval (0–1). This nonlinear transformation enhanced contrast around the stability threshold (FS ≈ 1) and improved visual separation between lower- and higher-stability samples (Figure 4c). The shape of the resulting distribution reflects the mathematical properties of the sigmoid function rather than a discrete physical boundary and is therefore used here primarily as a feature transformation for subsequent modelling rather than a direct physical interpretation.

Relationship between FS and geology

FS values exhibit systematic contrasts among geotechnical/material groups across the study area. Lithological units are reported using their dominant near-surface material descriptors extracted at the sampled locations from the QMAP-based classification. These descriptors represent mapped material expressions rather than laboratory-tested soil or rock units. FS values are shown on a log-transformed scale (log (1 + FS)) to reduce skewness and improve visual comparability across groups (Figure 5). Boxes represent the interquartile range, with the median indicated by the central line. Groups are ordered by increasing median FS (from less stable to more stable).

Weak and highly degraded materials, particularly weathered rock, sand, and unclassified units, display the lowest stability overall. These groups exhibit median FS values close to or below unity (0.80-1.01) and a high proportion of sampled locations with FS < 1, exceeding 49% and reaching over 70% for weathered rock. Under the adopted infinite-slope formulation, these low FS values reflect the combined influence of relatively low assigned shear-strength parameters and increased sensitivity to slope angle and saturation effects.

Materials with greater cohesion and/or frictional resistance, including stiff clay, clay, soft clay, and gravel, show substantially higher median FS values (1.45-2.55), with fewer than ~11% of sampled locations falling below the FS = 1 threshold. These contrasts highlight the role of material strength and drainage behaviour

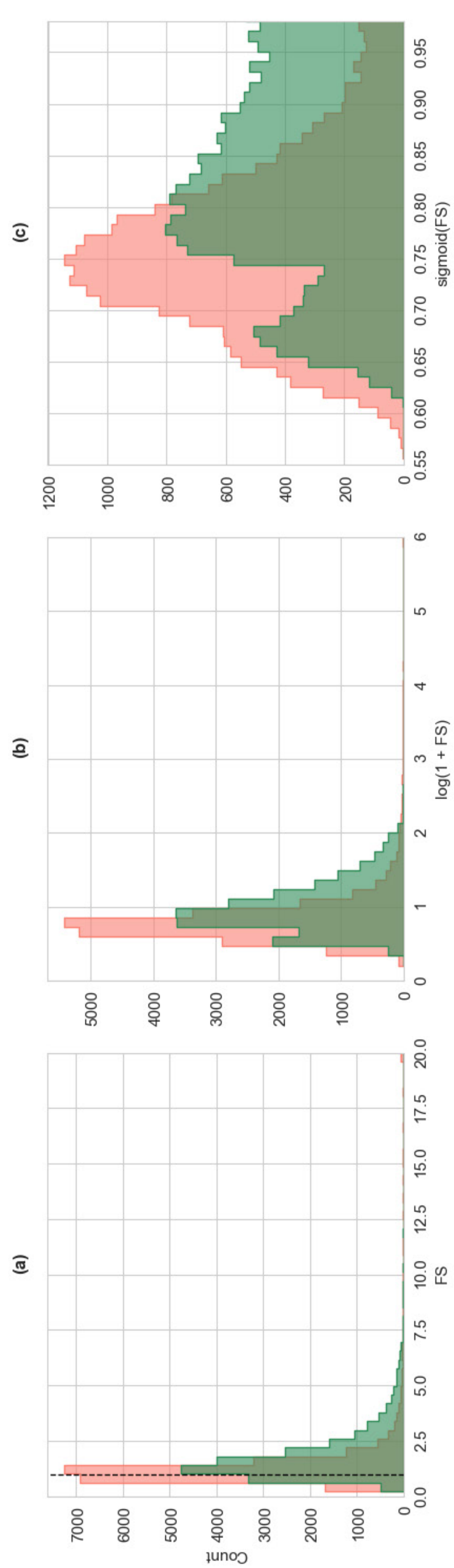

FIGURE 4: Distributions of FS values for landslide (red) and non-landslide (green) samples using (a) raw FS, (b) log-transformed FS, and (c) sigmoid-transformed FS. The dashed line in panel (a) marks the stability threshold (FS = 1).

in controlling slope stability within the assigned geotechnical parameter ranges.

Volcanic ash exhibits the highest overall stability, with consistently elevated FS values and no sampled locations falling below FS < 1. This behaviour reflects the combination of low unit weight and relatively high friction angles assigned to this material class, as well as its typical occurrence on gentler slopes within the study area.

Overall, the observed lithological contrasts are consistent with the expected response of the infinite-slope model to the adopted literature-based geotechnical parameterisation. While these patterns do not constitute independent validation, they provide a qualitative consistency check that the assigned parameter ranges produce geologically plausible stability patterns at the scale of the sampled locations.

Relationship between FS and slope / hydrological setting

FS values exhibit a clear and physically coherent dependence on slope angle and hydrological setting across the sampled locations. The inverse relationship between slope and stability follows the expected behaviour of the infinite-slope formulation, with FS decreasing systematically as slope angle increases.

To distinguish continuous model behaviour and quantitative instability summaries, Figure 6 illustrates the continuous relationship between slope angle and FS. At gentle slopes (<10°), sampled locations are almost entirely stable, with virtually no points registering FS < 1. FS values decrease progressively with increasing slope, and the spread of FS values widens notably between 10° and 25°, reflecting increasing sensitivity to small changes in slope angle under the infinite-slope model (Figure 6). A rapid transition to predominantly unstable conditions occurs at slopes exceeding approximately 25–30°, where the majority of sampled locations fall below the FS = 1 threshold.

The joint dependence of FS on slope angle and hydrological position reinforces the physical realism of the infinite-slope formulation implemented in this study. Steep, wet, and topographically convergent settings consistently exhibit the lowest FS values and the highest likelihood of shallow instability, whereas gentle, well-drained slopes remain overwhelmingly stable under the assumed conditions.

Comparison with Landslide Inventory (Qualitative Validation)

FS values derived from the infinite-slope model show a clear and meaningful separation between mapped landslide locations and non-landslide reference points. Across the case study dataset, landslide locations exhibit systematically lower FS values than non-landslide locations, indicating reduced stabilising shear resistance relative to driving stresses. The median FS at landslide locations is 1.13, compared to 1.55 for non-landslide reference points, with mean FS values of 1.38 and 1.89, respectively. This separation is further reflected in the proportion of sampled locations falling below the theoretical failure threshold (FS = 1), where 36.9% of landslide locations are classified as unstable, compared to 18.2% of non-landslide reference locations. These percentages were computed directly from the sample-point dataset as the proportion of locations with FS < 1 in each class.

Landslide locations are concentrated closer to the theoretical failure threshold (FS = 1), whereas non-landslide locations generally exhibit higher FS

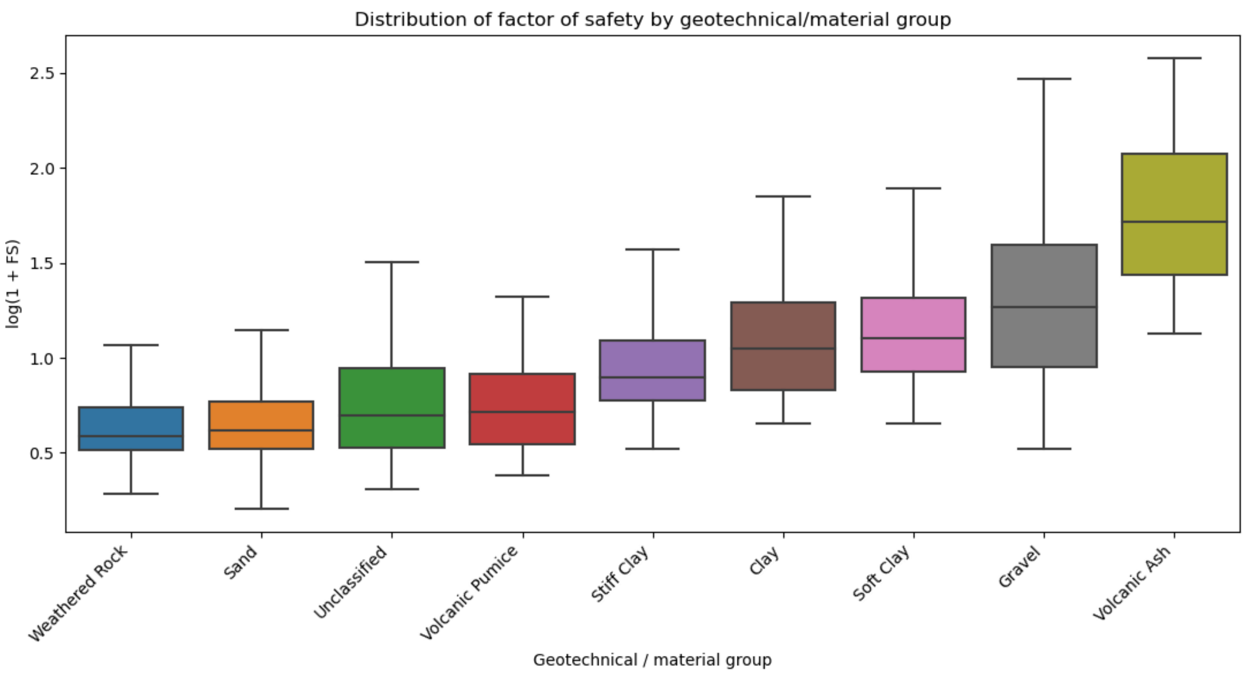

FIGURE 5: Distribution of FS by geotechnical/material group

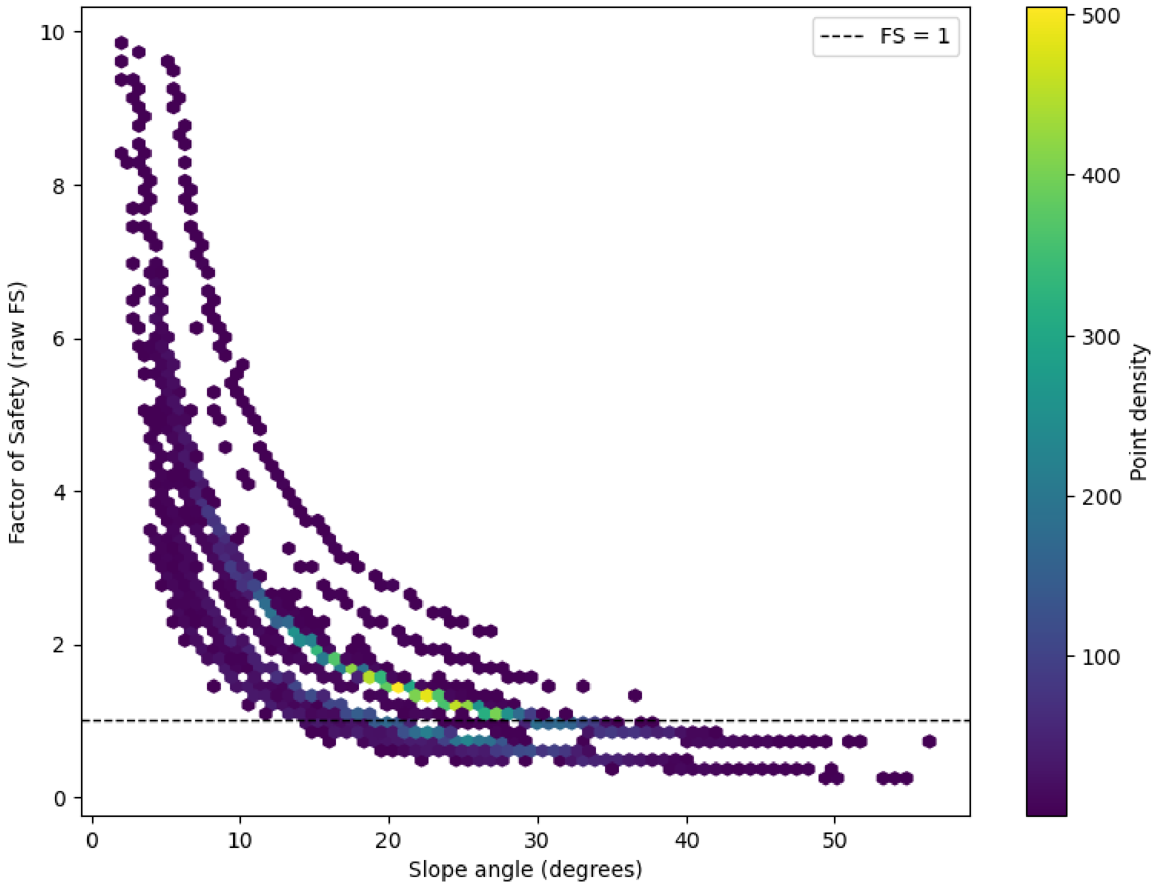

FIGURE 6: Relationship between FS and slope angle at sampled locations in the case study area.

values and broader distributions toward more stable conditions. This pattern is consistent with the expected physical behaviour of shallow landsliding, which preferentially occurs on steeper slopes, in weaker near-surface materials, and under hydrological conditions that promote elevated pore pressures. Although the available landslide inventory is incomplete and does not capture all shallow failures within the region, the observed descriptive separation between landslide and non-landslide reference locations indicates that the GIS- and literature-derived FS model assigns systematically lower stability to known failure sites. This qualitative agreement, obtained without site-specific geotechnical measurements, supports the use of the FS layer as a regional-scale screening tool and demonstrates its potential for broader susceptibility assessment applications.

Sensitivity analysis

The sensitivity-analysis results are shown in Table 4. The saturation ratio (s) exerted the strongest control on both mean FS and the proportion of unstable terrain. Increasing (s) from dry (s = 0) to fully saturated conditions (s = 1) produced a pronounced and non-linear increase in instability across the study area. Under dry conditions (s = 0), fewer than 1% of sample points exhibited FS < 1 across all soil-depth scenarios. At moderate saturation (s = 0.5), the proportion of unstable points increased to approximately 5-6%. Under fully saturated conditions (s = 1), instability increased sharply, with approximately 18-21% of points falling below the FS = 1 threshold.

This behaviour is consistent with infinite-slope mechanics, whereby increasing pore-water pressure reduces effective normal stress and shear resistance, shifting marginally stable slopes into failure. The strong sensitivity of slope stability to soil saturation highlights the importance of hydrological loading as a key control on shallow landslide initiation, consistent with the rainfall-triggered nature of landsliding observed in New Zealand hill-country environments. The strong sensitivity of FS to the saturation ratio s aligns with the dominant role of pore-pressure in triggering shallow failures (Montgomery & Dietrich 1994; Baum et al. 2008).

Soil depth had a secondary but systematic influence on FS. Increasing z from 0.5 m to 1.5 m resulted in a consistent reduction in mean FS across all saturation states, reflecting the linear increase in driving shear stress associated with thicker soil mantles. However, the magnitude of this effect was modest compared to that of hydrological saturation. For example, at s = 0.5, mean FS decreased from 6.7 to 3.3 as soil depth increased across the tested range, while the proportion of unstable points increased only slightly from 5.7% to 6.0%. A similar

TABLE 4: Summary of sensitivity-analysis results showing the influence of saturation ratio (s) and soil depth (z) on mean FS and the proportion of unstable points (FS < 1).

Saturation ratio (s)	Soil depth z (m)	Mean FS	Points with FS < 1 (%)
0.0	0.5	7.2	0.9
0.0	1.0	4.7	0.9
0.0	1.5	3.8	0.9
0.5	0.5	6.7	5.7
0.5	1.0	4.2	5.7
0.5	1.5	3.3	6.0
1.0	0.5	6.2	18.5
1.0	1.0	3.6	20.2
1.0	1.5	2.8	20.8

pattern was observed under fully saturated conditions (s = 1), where mean FS declined with increasing depth, but instability percentages changed by only a few percentage points.

These results indicate that soil thickness primarily influences FS through mechanical loading, while hydrological forces govern whether sample points cross the instability threshold. The near-linear response to z contrasts with the non-linear response to s, reinforcing the interpretation that pore-pressure effects dominate regional-scale stability patterns.

Taken together, the sensitivity analysis reveals three key insights: (a) hydrological forcing is the primary control on shallow slope instability, with FS responding strongly and non-linearly to increasing saturation, (b) soil depth exerts a moderate but predictable influence, primarily affecting mean FS without fundamentally altering the proportion or spatial pattern of unstable terrain, and (c) the infinite-slope formulation behaves in a physically consistent manner, exhibiting stronger sensitivity to pore-pressure-related parameters than to geometric assumptions.

Discussion

The results of this case study demonstrate that the GIS- and literature-based infinite-slope FS model produces physically coherent and geomorphically consistent patterns of shallow slope stability across the study area. Spatially, low FS values are concentrated on steep hillslopes, topographically convergent terrain, and channel-adjacent settings, while gentle, well-drained slopes are overwhelmingly stable under the assumed conditions.

Quantitative analysis confirms the dominant control of slope angle on stability, with FS decreasing systematically as slope increases and a rapid transition to unstable conditions occurring at slopes exceeding approximately 25–30°. Hydrological position further modulates stability on intermediate slopes, where wetter locations consistently exhibit a higher proportion of FS < 1 relative to better-drained terrain. At the steepest gradients, instability becomes nearly universal, indicating slope-dominated control that overwhelms hydrological modulation.

Comparison with the mapped landslide inventory used in the case study provides qualitative validation of the model behaviour. Mapped landslide locations are associated with systematically lower FS values than non-landslide reference points, with lower median FS and a substantially higher proportion of locations falling below the theoretical failure threshold. Although the available inventory is incomplete and does not capture all shallow failures, the observed statistical separation demonstrates that the FS model provides meaningful physical discrimination between more and less failure-prone terrain without site-specific geotechnical calibration.

The strength of the approach is fully reproducible and GIS-based: All inputs, including QMAP lithology, S-map soil properties, NIWA rainfall surfaces, and the LINZ 8-m DEM, are publicly available at national scale. Because all preprocessing, parameter assignment, and FS calculations were implemented in Python, the workflow can be repeated over any region in New Zealand without manual tuning, enabling consistent landslide screening in data-limited settings.

Physically meaningful geotechnical parameterisation: Assigning ϕ', c', and γ from published New Zealand sources ensures that parameter ranges are grounded in field and laboratory evidence, even though no site-specific shear tests were conducted. The stability contrasts observed between mudstone, colluvium, sandstones, and stronger rock units support that literature-derived values reproduce geologically realistic behaviour.

Overall, these results support the use of the FS layer as a regional-scale screening tool for shallow landslide susceptibility. The physically interpretable nature of the model, combined with its ability to capture first-order controls on instability using widely available GIS datasets, makes it suitable for broader regional susceptibility assessment applications. The workflow enables: (a) locating slopes that are likely to become unstable during wet periods, (b) identifying “critical” terrain for operational caution during harvesting or road construction, (c) examining how increased saturation after storms may shift stability thresholds, and (d) map terrain sensitivity before and after harvest activities.

A key finding of this study is that the infinite-slope FS is dominated by hydrological forcing particularly through rainfall-driven pore-pressure dynamics, which control transient reductions in shear resistance. Because hydrological proxies (rainfall, drainage proximity, soil drainage class) are well mapped national scales, spatial patterns of FS can be reasonably approximated at regional scales even in the absence of detailed site-specific geotechnical data. This is consistent with earlier theoretical and modelling frameworks (Dietrich & Montgomery 1998; Iverson 2000), which emphasise the role of hydrologically driven pore-pressure response in controlling shallow landslide initiation.

The proposed workflow aligns conceptually with the family of infinite-slope–based stability models but differs in complexity and data requirements. Classical infinite-slope formulations (Wu & Sidle 1995; Iverson 2000) require the same core parameters (c', ϕ', γ, z, m), but their implementation often depends on site-specific measurements. SHALSTAB (Montgomery & Dietrich 1994) couples infinite-slope mechanics with steady-state hydrology to represent subsurface convergence; however, it requires transmissivity and rainfall-intensity inputs that are rarely available at regional scale. SINMAP (Pack et al. 1998) incorporates parameter uncertainty through ranges of c', ϕ', γ, and s, producing a stability index rather than a single FS value. TRIGRS (Baum et al. 2008) provides transient modelling of infiltration and pore-pressure diffusion, but demands hydraulic conductivity, diffusivity, and detailed rainfall time series. The present workflow offers a lightweight, GIS-informed alternative that retains essential shallow-failure physics while remaining feasible for large, data-limited regions, an issue frequently highlighted in regional landslide studies (e.g., Ye et al. 2025). However, there are known limitations to the approach. These include:

- Literature-derived geotechnical parameters are appropriate for regional assessments, but they cannot capture local weakening due to intense weathering, roots, reworking, or micro-scale heterogeneity.
- The infinite-slope model assumes parallel flow and uniform saturation, and does not simulate transient infiltration, lateral convergence, perched water tables, or preferential flow through fractures or roots. As a result, true storm-driven pore-pressure dynamics may differ from the steady-state assumptions used here.
- New Zealand does not have a national-scale soil-depth map; therefore, z must be specified through scenario-based assumptions. Although sensitivity results show that z influences FS less strongly than s, uncertainty in soil depth remains a limitation for detailed site-scale assessments.
- Slope and curvature are sensitive to DEM quality. While the LINZ 8-m DEM is appropriate for regional evaluation, higher-resolution LiDAR would improve representation of convergent flow paths and shallow hollows.
- The study used a pointwise internal comparison between landslide and non-landslide samples, not an independent inventory. Although FS values showed the expected separation between the two groups, the lack of external validation limits the assessment of generalisation. Shallow landslides in plantation forests commonly originate on steep, fine-grained Tertiary sediments exposed during or after harvest and triggered by intense rainfall.

Conclusions

This study presented a reproducible, GIS- and literature-based workflow for estimating the FS in regions where site-specific geotechnical measurements are unavailable. By integrating national geological and soil datasets with DEM-derived terrain attributes and rainfall-driven hydrological proxies, the workflow enables large-scale, spatially consistent assessment of shallow landslide susceptibility. All processing steps, from parameter assignment to FS computation, were implemented programmatically, ensuring transparency and repeatability. The method captures major controls on shallow landslides in New Zealand hill-country and produces results consistent with established theoretical expectations and patterns reported in prior studies.

The resulting FS patterns aligned closely with the theoretical behaviour of the infinite-slope model. In particular, the sensitivity analysis showed that hydrological forcing, expressed through the saturation ratio s, exerts the strongest control on stability, with instability rates rising from <1% under dry conditions to ~20% under full saturation. Variations in soil depth and mechanical parameters produced comparatively modest changes, reinforcing the dominant influence of pore-pressure on shallow failures in hill-country terrain. Although the approach does not replace detailed field investigations, it provides a practical and scalable method for regional screening, especially in steep, erosion-prone landscapes where direct measurements are rarely feasible.

List of abbreviations

DEM: Digital Elevation Model
EPSG: European Petroleum Survey Group
FS: Factor of Safety
GIS: geographic information system
LiDAR: light detection and ranging
LINZ: Land Information New Zealand
NIWA: National Institute of Water and Atmospheric Research
NZTM2000: New Zealand Transverse Mercator 2000
QMAP: Geological Map of New Zealand at 1:250,000 scale
SHALSTAB: Shallow Landslide Stability model
SINMAP: Stability Index Mapping
TRIGRS: Transient Rainfall Infiltration and Grid-Based Regional Slope-Stability model
VCSN: Virtual Climate Station Network.

Competing interests

The authors declare that they have no competing interests.

Authors' contributions

MH conceived and designed the study, developed and implemented the Python-based workflow, processed and analysed the data, interpreted the results, prepared the figures, and drafted the manuscript. RV supervised the research, contributed to the study design and interpretation of the results, and critically reviewed and edited the manuscript. Both authors read and approved the final manuscript.

Acknowledgements

The authors gratefully acknowledge Forest Growers Research (FGR), Harvesting Automation & Robotics, for providing financial support for this research. The authors thank the anonymous reviewer for their constructive comments, which helped improve the manuscript.

Funding

This research was financially supported by Forest Growers Research, Harvesting Automation & Robotics. The authors retained responsibility for the study design, data analysis and interpretation, and preparation of the manuscript.

References

Baum RL, Savage WZ, Godt JW. 2008. TRIGRS: A Fortran program for transient rainfall infiltration and grid-based regional slope-stability analysis, version 2.0 (p. 75). Reston, VA, USA: US Geological Survey. https://doi.org/10.3133/ofr20081159

Baum RL, Godt JW, Savage WZ. 2010. Estimating the timing and location of shallow rainfall-induced landslides using a model for transient, unsaturated infiltration. Journal of Geophysical Research: Earth Surface, 115(F3), F03013. https://doi.org/10.1029/2009JF001321

Beven KJ, Kirkby MJ. 1979. A physically based, variable contributing area model of basin hydrology. Hydrological Sciences Bulletin, 24(1), 43-69. https://doi.org/10.1080/02626667909491834

Carter M, Bentley SP. 1991. Correlations of soil properties. Pentech Press, London, UK.

Chae BG, Park HJ, Catani F, Simoni A, Berti M. 2017. Landslide prediction, monitoring and early warning: A concise review of state-of-the-art. Geosciences Journal, 21(6), 1033-1070. https://doi.org/10.1007/s12303-017-0034-4

Dahal RK, Lombardo L. 2024. Towards physics-informed neural networks for landslide prediction. Engineering Geology, 344, 107852. https://doi.org/10.1016/j.enggeo.2024.107852

Dietrich WE, Montgomery DR. 1998. SHALSTAB: A digital terrain model for mapping shallow landslide potential. Technical report. National Council for Air and Stream Improvement, University of California, Berkeley, USA.

Duncan JM, Wright SG, Brandon TL. 2014. Soil strength and slope stability. 2nd ed. John Wiley & Sons, Hoboken, NJ, USA.

Fiolleau S, Falco N, Dafflon B, Uhlemann S. 2022. Improving slope stability estimates by incorporating geophysical and remote sensing monitoring data into hydro-geomechanical modelling. EarthArXiv preprint. https://doi.org/10.31223/X5CH2R

Froude MJ, Petley DN. 2018. Global fatal landslide occurrence from 2004 to 2016. Natural Hazards and Earth System Sciences, 18(8), 2161-2181. https://doi.org/10.5194/nhess-18-2161-2018

Hashemi M, Visser R. 2026. Hybrid landslide susceptibility modelling for rainfall-triggered landslides in forested slopes; a review for bridging physics-based and machine learning methods. New Zealand Journal of Forestry Science, 56: 9. https://doi.org/10.33494/nzjfs562026x480x

Hungr O, Leroueil S, Picarelli L. 2014. The Varnes classification of landslide types, an update. Landslides, 11(2), 167-194. https://doi.org/10.1007/s10346-013-0436-y

Iverson RM. 2000. Landslide triggering by rain infiltration. Water Resources Research, 36(7), 1897-1910. https://doi.org/10.1029/2000WR900090

Lilburne LR, Hewitt AE, Webb TH. 2012. Soil and informatics science combine to develop S-map: a new generation soil information system for New Zealand. Geoderma, 170, 232-238. https://doi.org/10.1016/j.geoderma.2011.11.012

Lindsay JB. 2016. Whitebox GAT: a case study in geomorphometric analysis. Computers & Geosciences, 95, 75-84. https://doi.org/10.1016/j.cageo.2016.07.003

Look BG. 2007. Handbook of geotechnical investigation and design tables. Taylor & Francis/Balkema, Leiden, The Netherlands. https://doi.org/10.1201/9780203946602

Marden M. 2012. Effectiveness of reforestation in erosion mitigation and implications for future sediment yields, East Coast catchments, New Zealand: A review. New Zealand Geographer, 68(1), 24-35. https://doi.org/10.1111/j.1745-7939.2012.01218.x

Marden M, Rowan D. 1993. Protective value of vegetation on Tertiary terrain before and during Cyclone Bola, East Coast, North Island, New Zealand. New Zealand Journal of Forestry Science, 23(3), 255-263.

Marden M, Rowan D, Watson A. 2023. Effect of changes in forest water balance and inferred root reinforcement on landslide occurrence and sediment generation following *Pinus radiata* harvest on Tertiary terrain, eastern North Island, New Zealand. New Zealand Journal of Forestry Science, 53: 4. https://doi.org/10.33494/nzjfs532023x216x

Montgomery DR, Dietrich WE. 1994. A physically based model for the topographic control on shallow landsliding. Water Resources Research, 30(4), 1153-1171. https://doi.org/10.1029/93WR02979

O'Loughlin EM. 1986. Prediction of surface saturation zones in natural catchments by topographic analysis. Water Resources Research, 22(5), 794-804. https://doi.org/10.1029/WR022i005p00794

Pack RT, Tarboton DG, Goodwin CN. 1998. The SINMAP approach to terrain stability mapping. In D Moore, O Hungr (Eds), 8th Congress of the International Association of Engineering Geology, Vancouver, British Columbia, Canada, Vol. 2, pp. 1157-1166. A.A. Balkema Publishers, Cape Town, South Africa.

Pei T, Qiu T. 2024. Landslide susceptibility mapping using physics-guided machine learning: A case study of a debris flow event in Colorado Front Range. Acta Geotechnica, 19(10), 6617-6641. https://doi.org/10.1007/s11440-024-02384-y

Petley DN. 2012. Global patterns of loss of life from landslides. Geology, 40(10), 927-930. https://doi.org/10.1130/G33217.1

Phillips C, Marden M, Basher L. 2012. Plantation forest harvesting and landscape response - what we know and what we need to know. New Zealand Journal of Forestry, 56(4), 4-12.

Phillips C, Betts H, Smith HG, Tsyplenkov A. 2024. Exploring the post-harvest 'window of vulnerability' to landslides in New Zealand steepland plantation forests. Ecological Engineering, 206, 107300. https://doi.org/10.1016/j.ecoleng.2024.107300

Sharma S. 2002. Slope stability concepts. In Abramson LW, Lee TS, Sharma S, Boyce GM, Slope stability and stabilization methods. 2nd ed. John Wiley & Sons, New York, USA. pp. 329-454.

Sidle RC, Bogaard TA. 2016. Dynamic earth system and ecological controls of rainfall-initiated landslides. Earth-Science Reviews, 159, 275-291. https://doi.org/10.1016/j.earscirev.2016.05.013

Skempton AW, DeLory FA. 1957. Stability of natural slopes in London Clay. In: Proceedings of the 4th International Conference on Soil Mechanics and Foundation Engineering, London, UK, Vol. 2, pp. 378-381.

Smith HG, Neverman A, Betts H, Spiekermann R. 2023. The influence of spatial patterns in rainfall on shallow landslides. Geomorphology, 437, 108795. https://doi.org/10.1016/j.geomorph.2023.108795

Smith S, Visser R, Bloomberg M, Palmer D. 2024. Methods for ascertaining shallow landslide susceptibility in the harvest planning process. New Zealand Journal of Forestry, 68(4), 38-45.

Tait A, Henderson R, Turner R, Zheng X. 2006. Thin plate smoothing spline interpolation of daily rainfall for New Zealand using a climatological rainfall surface. International Journal of Climatology, 26(14), 2097-2115. https://doi.org/10.1002/joc.1350

Wang Y-H, Wang L-Q, Zhang W-G, Liu S-L, Sun W-X, Hong L, Zhu Z-W. 2024. A physics-informed machine learning solution for landslide susceptibility mapping based on three-dimensional slope stability evaluation. Journal of Central South University, 31(11), 3838-3853. https://doi.org/10.1007/s11771-024-5687-3

Wu W, Sidle RC. 1995. A distributed slope stability model for steep forested basins. Water Resources Research, 31(8), 2097-2110. https://doi.org/10.1029/95WR01136

Ye C, Wu H, Oguchi T, Tang Y, Pei X, Wu Y. 2025. Physically based and data-driven models for landslide susceptibility assessment: Principles, applications, and challenges. Remote Sensing, 17(13), 2280. https://doi.org/10.3390/rs17132280